Journal of Energy Storage 32 (2020) 101735

Contents lists available at ScienceDirect

Journal of Energy Storage

journal homepage: www.elsevier.com/locate/est

Synthesis of porous carbon nanostructure formation from peel waste for low cost flexible electrode fabrication towards energy storage applications

Jothi Ramalingam Rajabathar[a,*], Sivachidambaram Manoharan[b,c], Judith Vijaya J[b,*], Hamad A. Al-Lohedan[a], Prabhakarn Arunachalam[a]

[a] Chemistry Department, College of Science, King Saud University, Riyadh 11451, Saudi Arabia
[b] Catalysis and Nanomaterials Research Laboratory, Department of Chemistry, Loyola College (Autonomous), Chennai 600 034, India
[c] Department of Chemistry, Theivanai Ammal College for Women, Villupuram- 605602, Tamilnadu, India

ARTICLE INFO

Keywords:
Carbon nanoparticle
Pyrolysis
Renewal energy
Biowaste
Jackfruit
Supercapcitor

ABSTRACT

Porous activated nanostructure carbon is prepared by feasible two steps method utilizing naturally available bio-wastes such as jack fruit peel waste (JFW) and studied the effect of pyrolysis condition for porosity formation. X-ray analysis and BET pore size analysis confirmed the formation of graphitic nature carbon with micro and mesoporous existence. HR-SEM and TEM images of Jack fruit (JF) derived porous carbon samples are shown spherical nanoball and tiny nanotube morphology. High resolution SEM images further confirms that the, increase in the activation temperature increase the uniform hexagon shape porous structure formation. The superior electrochemical activity and recycling stability was achieved for our method prepared (phohphoric acid activation method using graphite crucible mold) porous carbon materials. The Cs (specific capacitance) of the JF-9 (porous carbon prepared Jack fruit at 900 °C) sample was shown 324 F/g at the scan rate of 5 mV/s using Na_2SO_4 electrolyte. The JF carbon sample exhibits a higher capacitance retention of 93% for upto 5000 cycles. We found that the JF derived porous carbon sample shows higher recycling capacity by Galvano static charge-discharge analysis. The effect of current density and scan rate on specific capacitance property are analyzed in detailed by cyclic-voltammetry , Galvano static charge-discharge method and electrochemical impedance spectroscopy analysis.

1. Introduction

The global huge energy demands are increaseing day by day due to the thrust on rapid development of domestic and industrial needs and a dreadful increase in the environmental pollution [1–3]. Preparation of porous activated nanocarbon (PAC) strongly depend on theprecursor material and the preparation method employed in its preparation process, such as activating agent mass ratio, concentration and temperature conditions [2–4]. The higher specific capacitance, long cycle life and low cost preparation method are the main objectives for proposing the most promising electrode materials for electrochemical double layer capacitance (EDLC) [4]. However, the commercially available porous carbon modified electrode materials for supercapacitor application are micropores with pore size <2.0 nm [5,7]. The poor capacitance retention especially at very high discharge rate, hindering their utilization for high power and high energy density super capacitor development. To overcome the above problem, hierarchical porous carbon having micro and mesopores are recently attracting to a improved supercapacitor electrode fabrication [8]. Among them, the mesopores can act as feasible ion-transportation channels for enhanced ion diffusion. The micropores serve as a high loading of accessible ion storage sites to enhance the capacitance. A great variety of raw materials with high carbon content and low amount of inorganic compounds are mainly used in the large-scale manufacture of porous nanocarbon, such as rice husk, fire wood and pistachio shells, bamboo, banana fibers, waste coffee beans, corn grains, cassava peel waste, sugar cane bagasse, and sunflower seed shells [6–8]. Nowadays, the production of porous nanocarbon from industrial and agricultural waste products are used in the active research, due to their controlled removal, minimization to prepare lower-cost PC and for potential applications [9–11].

Electric double layer playing an interesting role in supercapacitor device development and it has some specific properties to store energy electrostatically, such as highly porous materials with huge surface area and pore size distribution, thermal stability, and presence of electro-active surface functional groups, electrolyte and so forth [12,13]. On the other hand, the properties of the synthesiszed PC determine the

* Corresponding authors.
E-mail addresses: jrajabathar@ksu.edu.sa (J.R. Rajabathar), jjvijaya78@gmail.com (J.V. J).

https://doi.org/10.1016/j.est.2020.101735
Received 1 May 2020; Received in revised form 19 July 2020; Accepted 3 August 2020
2352-152X/ © 2020 Elsevier Ltd. All rights reserved.

electrochemical performance presents in the porous carbon with different morphological form for modified electrode applications [14,15].

To the best of our knowledge, there is no much publication related with the usage of jackfruit peel waste (JFW) as a precursor material for porous carbon production and only few reportes related with Jackfruite waste by Inbaraj and Sulochana [16]. They used sulphuric acid as an activating agent for fabricate the porous carbon electrode. The as prepared porous carbon act as good adsorption behaviour for Cd (II) removal. Jackfruit (JF) was originated from India and spread out into tropic regions. JF peels has no commerical value and often create a disposal problem for local environment. Recently, many research report related with multi porous carbon based modified electrode development from various low cost precursor materials for supercapcitor and lithium battery applications [17–20]. In the present study, JFW was activated by chemical activation method using phosphoric acid as an activating agent. Chemical activations also has better development towards a porous structure [20]. It has been found that both the surface area and porosity are greatly influenced by the preaparation condition, such as the activation time, activation temperature and impregnation ratio [21–22]. Nevertheless, it has been found that the ordinary (activating agent mixture-sample) chemical activation process was the best compared to physical and acid wash activation method [21]. Hence, we employed two-stage preparation of porous carbon formation by adopting low cost clay molded graphite crucible (CMGC) technique. Further, we activated at four different temperatures and it is characterized for structural, morphological, porous nature and electrochemical performance.

2. Experimental

2.1. Preparation of porous nanocarbons

Jackfruit peel waste (JFW) is the raw material used to prepare porous nanocarbons and it is collected from Villupuram district. Tamilnadu,India. The porous activated carbon is prepared by two stage processes. First step is the preparation of pre-carbonized carbon. The jackfruit peel waste raw material was cut in smaller pieces and washed for several times to remove the impurities like sand and other unwanted matters followed by dried for 24 h at 80°C. The dried raw material was transferred in a graphite crucible and sealed. The clay molded graphite crucible was placed in a muffle furnace (400°C for 4h), to create the vacuum conditions. Clay molded graphite crucible (GMGC) is sealed by heating for few minutes to generate maximum vacuum instead of heating under inert gas condition, which is not cost effective. Finally, the PCC sample was collected from the graphite crucible by crushing the molded clay using hammer and the sample was labelled as JF-PCC.

Second step is the preparation of PC by chemical activation method, 20 g of PCC was mixed with the activating agent, H_3PO_4 in the ratio of 1:4 and stirred for 3 h at 80°C. The abvoe prepared solution filltered followed by dried at 80°C for 24 h. The clay molded graphite crucible was further calcined at 600, 700, 800 and 900°C for 4 h under vacuum. After maintaining the temperature and fixed time, the clay molded graphite crucible was taken out of a muffle furnace and cooled at room temperature. Then the molded clay was broken in a graphite crucible and the sample was collected. All samples were washed for 3 to 4 times using distilled water to maintain a neutral pH = 7 and dried at 80°C for 24 h. Finally, the sample was collected and labelled as JF-6, JF-7, JF-8 and JF-9. Scheme 1 demonstrates the schematic diagram of the preparation of JFW porous nanocarbon (PC) or activated carbon (AC)

2.2. Characterization

The crystalline structure of porous activated carbon were analyzed by the X-ray diffraction (XRD) method (Bruker D8) and Cu Kα radiation source (λ = 1.5406 Å) was utilized in the scanning angle range of 10 to 90° at 10° min^{-1}. The Ft-IR analysis was carried out using Shimadzu

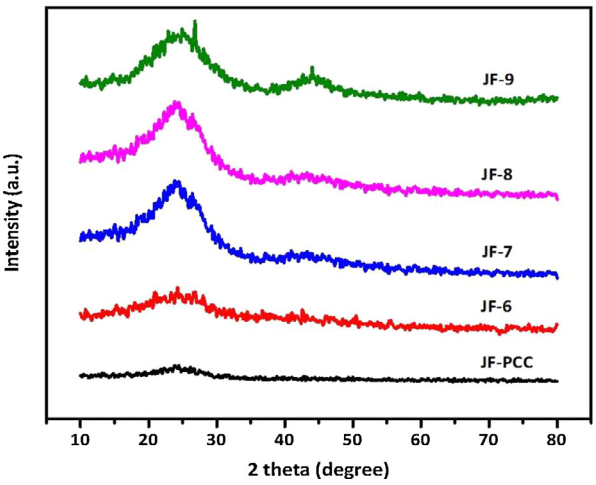

Fig. 1. X-ray diffraction patterns of (a) JF-PCC, (b) JF-6, (c) JF-7, (d) JF-8 and (e) JF-9 Porous carbon samples.

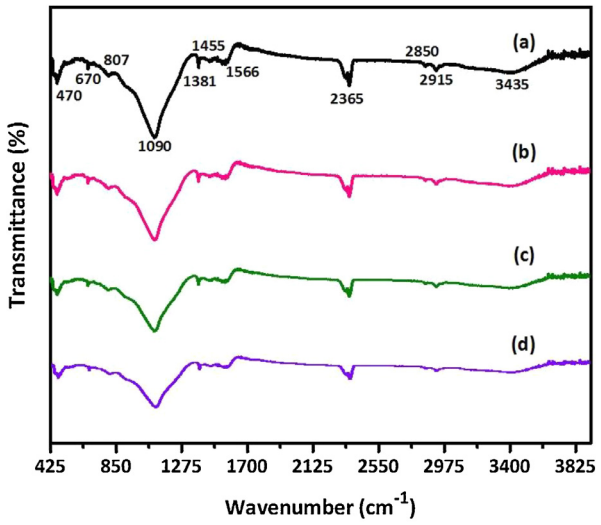

Fig. 2. FT-IR spectra of (a) JF-6, (b) JF-7, (c) JF-8, (d) JF-9 Porous carbon samples.

(FTIR-8400S) spectrophotometer. The spectral data of the porous carbon recorded in the wave number range from 400 cm^{-1} to 4000 cm^{-1}. The morphology and microstructure of the porous nanocarbon was studied using scanning electron microscope (JSM 6490-LV). High-resolution transmission electron microscopy was recorded using (FEI Tecnai G20) instrument. The surface area and pore size was analyzed by the nitrogen adsorption desorption isotherms using Micromeritics ASAP 2020 instrument at 77 K.

2.3. Modifed electrode fabrication and electrochemical measurements

The modified electrode (JF derived activated carbon based) was prepared by using 16 mg of as-prepared porous carbon with 2 mg of poly (vinylidene difluoride) binder was added to 2 mg of acetylene black to enhance the capacitive nature by avoiding the resistance of binder. N-methyl pyrrolidinone (1 to 2 mL) as an organic solvent is added to made a paste. The paste was coated in a square type nickel foil (1 × 1 cm) and it serves as a current collector. The electrochemical measurements of as-prepared porous nanocarbon modfied electrode was anayzed by the cyclicvoltammetry , Galvano static charge-discharge , electrochemical impedance spectroscopy. The effect of current density, scan rate and also tests the cyclic stability (5000 cycles) in 1M

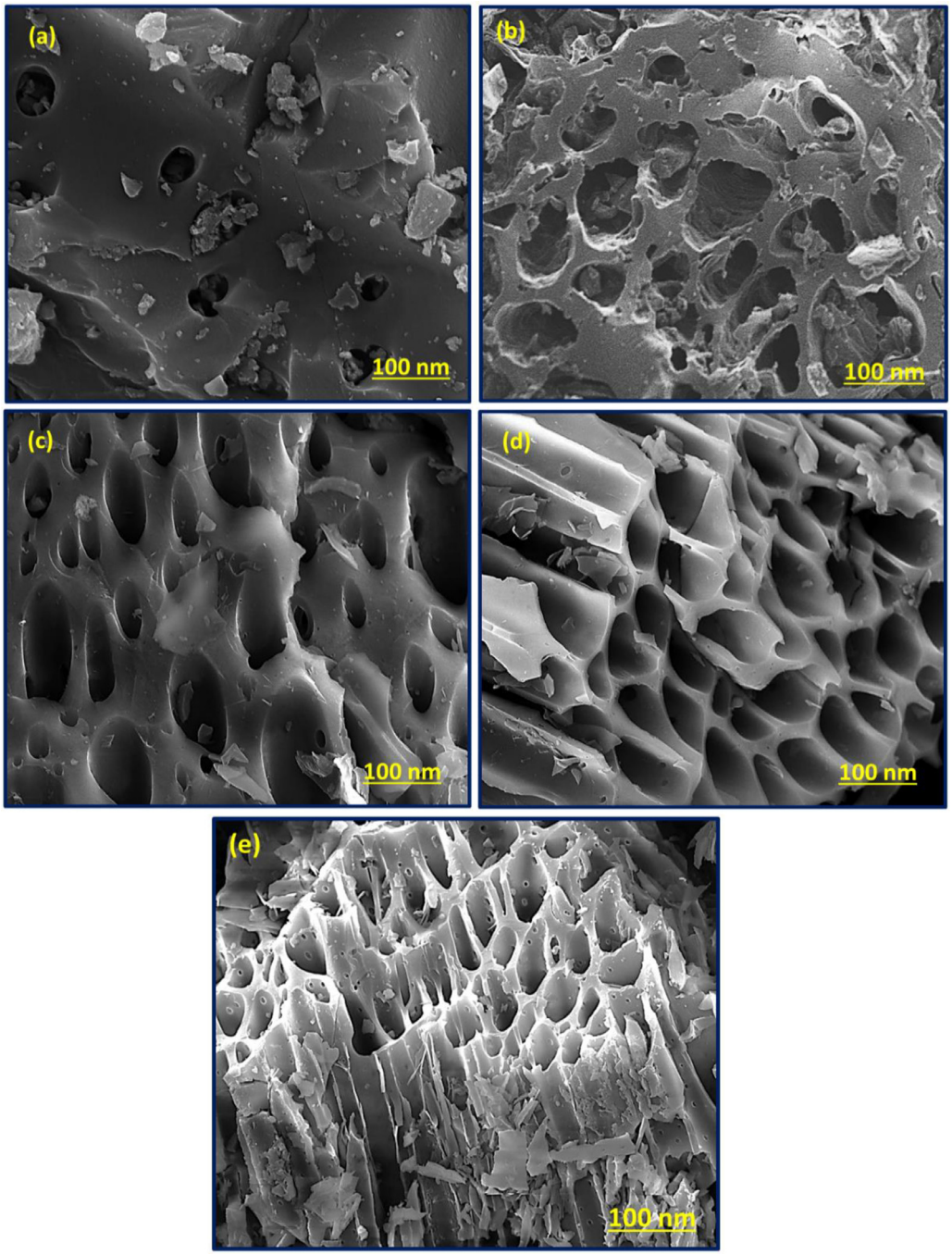

Fig. 3. HR-SEM micrographs of (a) JF-PCC, (b) JF-6, (c) JF-7, (d) JF-8 and (e) JF-9 Porous carbon samples.

Table 1.
Sample code, surface area, pore volume and average pore diameter of JF derived activated carbons.

Sample (JPW-AC)	S_{BET}[a] (m^2/g)	S_{micro}[b] (m^2/g)	S_{meso}[c] (m^2/g)	V_{micro}[d] (cm^3/g)	V_{meso}[e] (cm^3/g)	V_{Total}[f] (cm^3/g)
JF-6	689	492	197	0.301	0.194	0.495
JF-7	984	637	347	0.435	0.229	0.664
JF-8	1260	823	437	0.571	0.298	0.869
JF-9	1585	993	592	0.635	0.330	0.965

[a] BET surface area. [b]Micropore surface area. [c]Mesopore surface area. [d] Micropore volume. [e]Mesopore volume. [f] Total pore volume.

Na_2SO_4 electrolyte (Ametek PARSTAT 4000).

3. Results and discussions

3.1. X-ray diffraction studies

The XRD patterns of JFW derived porous carbon are shown in Fig. 1. Two peaks were identified at 2θ around 23° (100) and around 43° (101) [16]. The sharp peak at 26° (002) due to the presence of graphitic carbon. The reported graphitic carbon prepared by other activation process has matches very well with our results (JCPDS card number 75-2078) [23]. Generally, the prepared activated carbon was almost amorphous. The porous carbon prepared at low carbonizing temperature (400°C) had no broadening at 2θ around 23°. But the sharp peaks

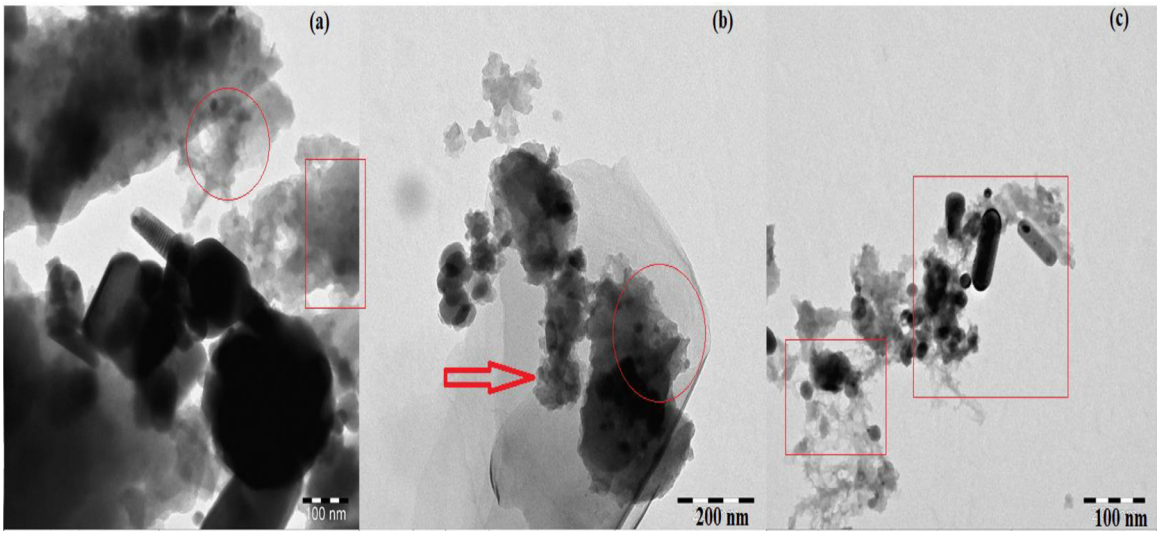

Fig. 4. HR-TEM micrographs of (a) JF-9 at 100 nm (b) JF-9 at 200 nm (c) JF-8 at 100 nm.

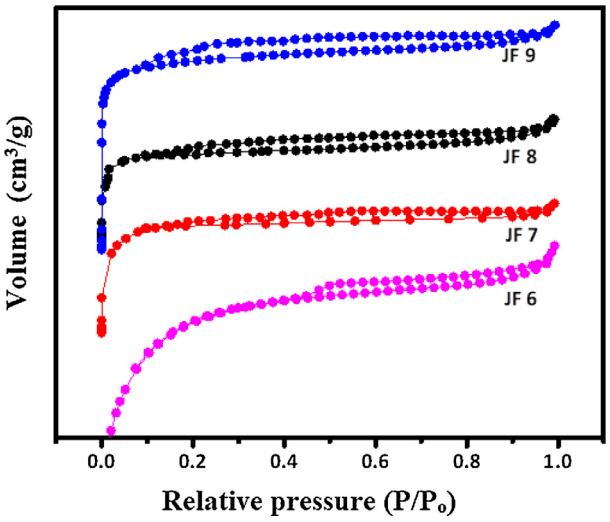

Fig. 5. Nitrogen adsorption-desorption isotherms of Synthesized Porous Carbon samples derived from Jackfruit waste.

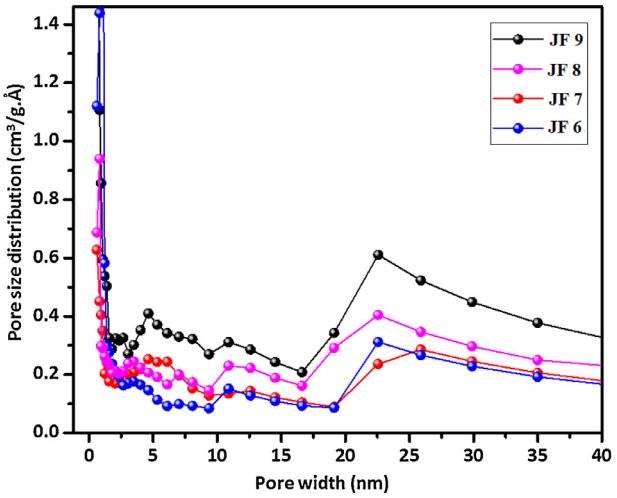

Fig. 6. Pore size distribution and analysis of Synthesized Porous Carbon samples derived from Jackfruit waste.

were obtained for the JF-9 samples at 26° and 43°, which showed that the JF-9 sample is more graphitic in nature than the other samples JF-8, JF-7 and JF-6. JF 6 is prepared at low activation temperature and it denotes the small broadening at 2θ around 23° because initial stages of porousityformation in the activation process. Further, at higher temperature the broadness and intensity of the peaks are increased at 2θaround 23° and 43°. Hence, we conclude that the activation temperature is playing important role in conversion of amorphous nature into graphitic carbon formation.

3.2. FT-IR studies

Fourier transform-infrared analysis is shown in Fig. 2 illustrates that the jackfruite derived porous nanocarbon JF-6, JF-7, JF-8 and JF-9. All samples are shows similar Ft-IR spectra and it indicates that all the samples are activated by H_3PO_4. The shoulder at 1090 cm^{-1} due to ionizedlinkage (P^+-O^-) in acid phosphate esters and symmetrical vibration from the chain of polyphosphate like P–O–P , similar kind of peak are observed for phosphoric acid activation method prepared porous carbon [21–24]. The absorption band at 1381 cm^{-1} due to C-O stretch and the functional groups Exists such as alcohol, carboxylic acid, esters and ethers. The peak at 3435 $cm^{-1}$and 750 cm^{-1} indicates the O-H, carboxylic group and Si-H bonds [25]. The peak at 1566 cm^{-1} belongs to the aromatic Carbon = Carbonstretching. The peak at 1455 cm^{-1} due to C-H of alkanes existence. The similar Ft-IR peaks obtained for most of the phosphoric acid activation method prepared nanoporous carbon [26]. The peak at 2330 cm^{-1} due to presence of -CH_2 functional group, which is confirmed by cited reference of phosphoric acid activated saw dust carbon [26].

3.3. Morphological studies

HR-SEM micrographs of the pre carbonized carbon (PCC) and synthesized porous carbon from JF waste are shown in Fig. 3 (a-e). The as-prepared JFW (PCC) porous carbon exhibited flatten-rough surface and no porosity on the surface is observed in Fig. 3a.

In Fig. 3(b), JF 6 depicts more smaller pores than JF 9 and it clearly indicates that JF 6 is exhibit as micro-porous comparatively JF 9 (Fig. 3e), which has enlargement in pores and it has both micro and mesoporosity. Similarly, JF 7 (Fig. 3c) has exhibited a smoother surface and less degree of porosity, than JF 9. The other samples (JF 7 and JF 8) are shows less hierarchical and irregular pores in the Fig. 3(c, d). The differences between the all JF porous carbon samples may be due to the usage of H_3PO_4 at higher activation temperature, and it reacts both the

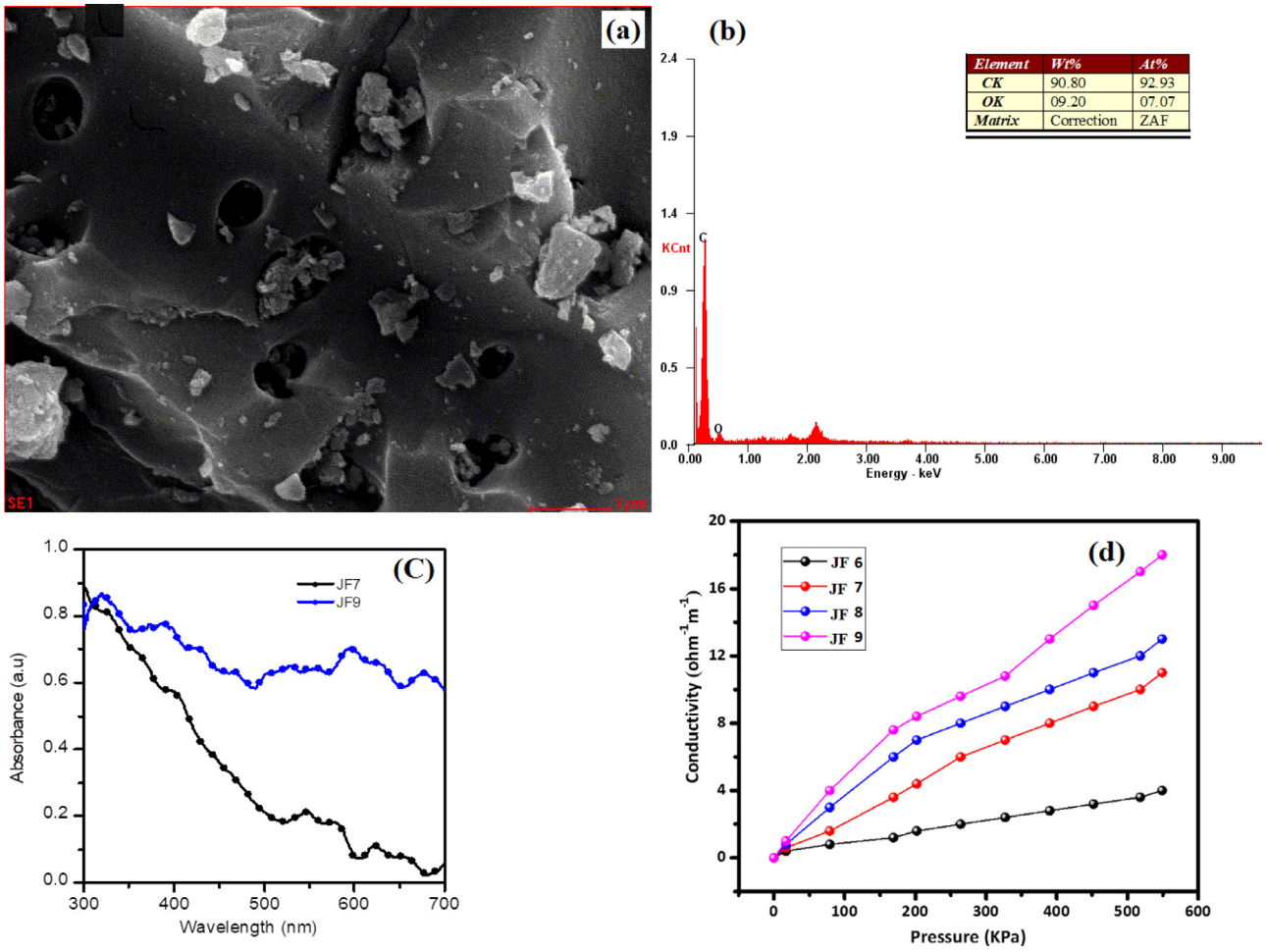

Fig. 7. (a-b) Elemental composition confirmation by SEM- EDX analysis of JF-9 porous carbon;(c) Absorption spectra of synthesized porous carbon (JF-7&9) from jackfruit sample; (d) Electrical conductivity of Porous Activated Carbon samples derived from Jackfruit waste.

interior-exterior surface and creates more pores in the JF 9 sample.

Cylindrical-like pores are exhibited as shown in Fig. 3(e), when it is activated at 900°C. More pores creation enhances the improvement in the surface area values and it is evident from Nitrogen adsorption-desorption isotherm analysis (Table 1). The JF-9 sample exhibits the pore channels that are interconnected with each other as shown in Fig. 3(e). The above results are justifying one for double layer capacitors, because the interconnected channels are main reason for charge transfer in EDCL [27,28].

Fig. 4 shows the HR-TEM analysis for morphological and structural studies of the JF-9 sample. Fig. 4a showed the spongy (square marked in red color in Fig. 4a) and glassy layered nanotube with spherical carbon nanoparticle formation for the as synthesized porous carbon samples (Fig. 4b-4c). The graphitic nature of JF-9 derived porous carbon samples was further largely magnified and it depicted the agglomeration of particle into spherical Nanoball shape and tiny nanotube like morphology formation occured as shown in Fig. 4c. The above type of interconnected spherical nanoball porous activated carbon could provide a identical open porous system [27]. The improved surface area with unique porous structure provide short diffusion path for incoming electrolyte ions [29].

3.4. Nitrogen adsorption–desorption isotherms

The pore structure and BET (Brunauer-Emmett-Teller) surface area parameters were evaluated from N_2 adsorption-desorption isotherms. Fig. 5 shows the Nitrogen adsorption-desorption isotherms at 77 K for JF-6, JF-7, JF-8 and JF-9 showing the BET surface area values such as 689, 984, 1260 and 1585 m^2/g (Table 1), respectively. JF-6 showed type I nitrogen isotherms, with respect to IUPAC classification, thus characterizing microporous property. JF-7, JF-8 and JF-9 showed a H-3type hysteresis loop, which is belong to typeIV isotherm based on IUPAC and it indicating the large amount of mixed micro and mesoporesity [30]. The isotherms presented a sharp increase of N_2 uptake at a very low relative pressure and forms the horizontal plateau for JF-6, which causes lower BET surface area vaues than JF-7, JF-8 and JF-9. The porous carbon (JF-9) shows larger and fine shape adsorption-desorption hysteresis loop than the all other samples in Fig. 5, which indicates that JF-9 has high micro and mesoporesity such as 0.635 and 0.330 cm^3/g. Table 1 shows the respective pore size for JF-6 (0.301 and 0.194 cm^3/g), JF 7 (0.435 and 0.229 cm^3/g) and JF 8 (0.571 and 0.298 cm^3/g). JF-9 shows the higher N_2 adsorption among other porous carbon, due to the higher surfacearea values and larger total porevolume values like 0.965 cm^3/g. In chemical activation using H_3PO_4 as the activating agent, at a higher temperature (900°C), the reaction between H_3PO_4 and carbon occurs [30,31]. Then, phosphorous will intercalate into complex carbon matrix, thus resulting in the brodening of the layers and increases the total pore volume [32]. At higher temperature condition, a maximum brodening of micro pores to mesopores occurs in activated porous carbon.

Fig. 6 shows the pore size distributions for the as prepared Jackfruite derived (JF-6, JF-7, JF-8 and JF-9) porous activated carbon samples. Most of the pores from JF-6 were < 2 nm. While the pore width range continued to increase, when the temperature increases.

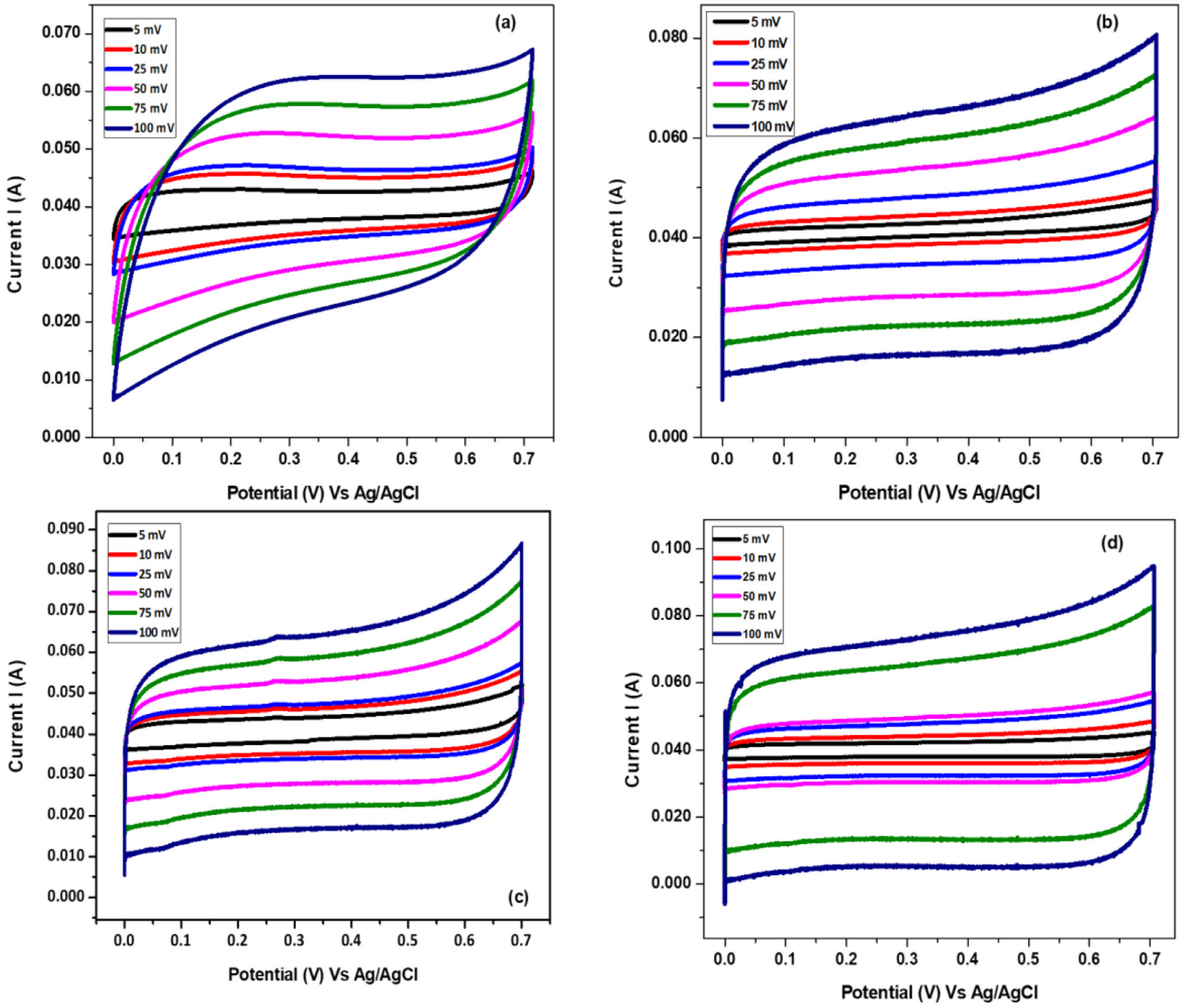

Fig. 8. Cyclic-voltammograms of (a) JF-6, (b) JF-7, (c) JF-8 and (d) JF-9 Porous carbon samples.

Table 2.
Experimentally calculated specific capacitance values of CV and GCD for JF-6, JF-7, JF-8 and JF-9 samples at different scan rate.

Samples	Specific capacitance from CV (F/g)							Specific capacitance from GCD (F/g)		
	5 mV/s	10 mV/s	20 mV/s	25 mV/s	50 mV/s	75 mV/s	100 mV/s	1 A/g	3 A/g	5 A/g
JF-6	168	155	142	126	111	102	88	165	142	120
JF-7	205	195	174	155	137	113	97	203	175	144
JF-8	268	242	223	206	181	162	136	294	256	213
JF-9	324	305	283	275	252	238	214	320	297	274

The above result further confirms that the H_3PO_4 activation process brings higher specific and improved surface area and total porevolume for JF-9 sample On the basis of the above results, it can be concluded that the JF-9 sample had a hierarchical porous structure with the interconnected micropores and mesopores. Such a porous structure is expected to improve the ion diffusion, and efficient to accumulate charge [33]. The enhanced surface area and higher porevolume of JF-9 sample would contribute to develop high charge storage, ion transport and it advantageous in capacitance performance when used in supercapacitor applications [34].

Fig. 7(a-b) shows elemental composition confirmation of jackfruit derived porous carbon prepared at high temperature (JF-9) by HR-SEM analysis, only two major peak are obtained for carbon content of (90.8 wt) and Oxygen content of (9.2 wt%) based on inset table in Fig. 7b. The EDX analysis is clearly confirms that the no other element formation, in other words high purity porous nanostructure carbon formation by graphite mold crucible heat treatment method (Scheme 1 at stage 2). Fig. 7(C) shows the Absorption spectra of as synthesized porous carbon particle dispersed in ethanol medium, the typical absorption region due to electronic transition between 300-400 nm is obtained. The absorption peak at 325 nm obtained for JF-9 and slight shift in peak observed for JF-7, the absorption peaks due to contributed from the π-π* electronic transition of C = C. Normal absorption region is between 180 nm-250 nm, longer shift in absorption associate with ethanol molecules absorbed to the surface of carbon particles and it generate the π-π interaction between the imidazolium rings of the ionic solvent. [35]. Absorption spectra is further confirms that the increase in calcination temperature playing the crucial role in the formation of orderly

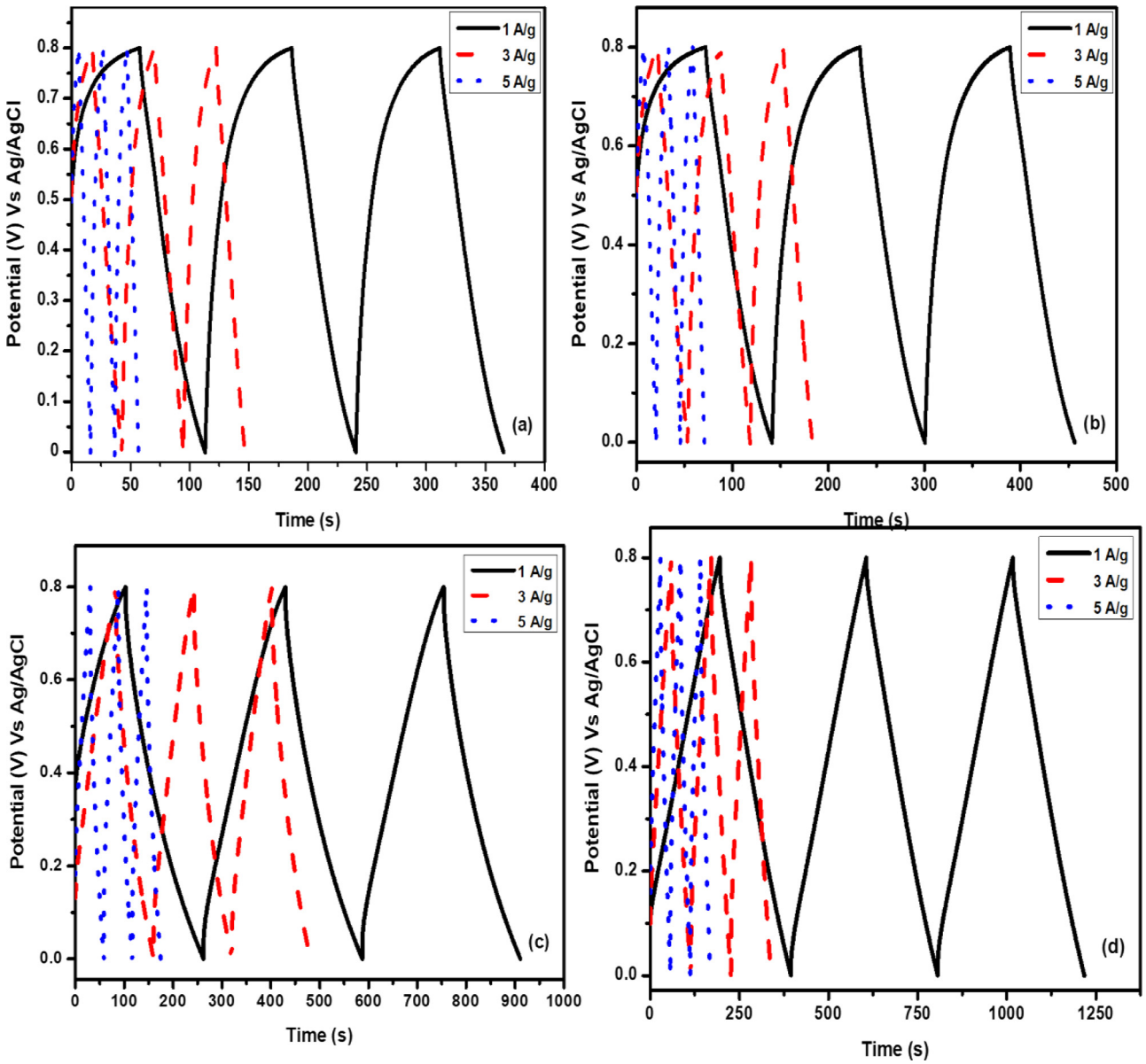

Fig. 9. Galvanostatic charge-discharge profiles of (a) JF-6, (b) JF-7, (c) JF-8 and (d) JF-9 Porous carbon samples.

arrangement of hierarchical pores in activated carbon. The excellent super capacitance performance is more connected to the higher conductivity, improved surfacearea and reasonable poresize distribution of the prepared porous carbon calcined at higher temperature(JF-9). Fig. 7d shows the conductivity measurement of the above mentioned JF carbon samples and the data indicates that the JF 9 samples have high electrical conductivity, because the JF 9 has higher BET surface area with hierarchical pores than other PAC samples. The hierarchical pores enhance the mobility of ions into the pores even faster to achieve the larger electrical conductivity.

4. Electrochemical characterizations

4.1. Cyclic voltammetry studies

Figure 8 shows the Cyclic-Voltammogram (CV) curves with potential window ranging from 0 to 0.68 V forJF-6, JF-7, JF-8 and JF-9 (Fig. 8 a-d)) at different scan rates of 5 mV/s to 100 mV/s. Generally, the ideal electrochemical active electrode material shows rectangular CV shape. The sample JF-6 and JF-7 shows a less and quasi rectangular shapes (Fig. 8a and b). Thus indicating their lesser super capacitive behavior. Higher porosity creates the improved performance at double layer formation electrostatically and that is the reason for displayed rectangular shapeCV curves of JF-8 and JF-9 (Fig. 8c and 8d). Surprisingly, nearly symmetrical box-like shape of CV curves obtained for JF-9 from Fig. 8d and it is demonstrating the ideal super capacitive performance. After the CV testing, specific capacitance calculated from the Eq. (1)

$$C_s = \int \frac{\Delta I}{2\,Vm(v_2 - v_1)} dV \qquad \text{i. e. } \Delta I = I_a - I_c \tag{1}$$

The calculated specific capacitance is given in Table 2. From the Table 2, C_s values are displayed at different san rates (5mV/s to 100 mV/s), when the scan rate increases, specfic capacitance values are decreases for all the Jackfruit derived porous carbon samples. At low scan rate of 5 mV/s, the JF-9 proves as a good charge propagation, fast ion diffusion within the pores and lesser contact-resistance and quick reorganizing of the electrical-double(ED) layer at the different potentials [36]. The above results indicated that the increase in calcination temperature increases the porosity rapidly from JF-6 sample to JF 9

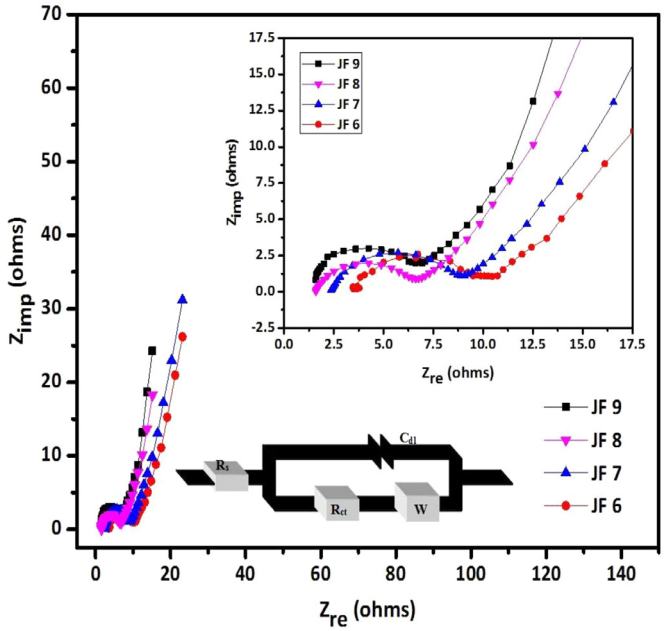

Fig. 10. Nyquist plot for Porous Carbon samples (sinusoidal signal of 5 mV) over the frequency range of 100 kHz to 1 mHz. Z_{re} is real impedance and Z_{imp} is imaginary impedance.

sample. Hence, JF-9 shows higher BET surface area value (1585 m^2/g) with large electrochemical storage.

4.2. Galvanostatic charge–discharge studies

In order to cross cheak the super-capacitance values and its electrochemical activity of the Jackfruite derived porous carbon was determined. Galvanotactic charge-discharge (GCD) analysis at different current densities such as 1 A/g , 3 A/gand 5 A/g is carried out and it shown in Fig. 9. All the JFW porous carbons provide the triangular shaped curve. In the case of JF-6 exhibits small slanting portion in the triangle at low current density (1 A/g) with a slight IR drop with low internal resistance [37]. Similarly, JF-7 and JF-8 sample has very little slanting portion and it shows small internal resistance. But, JF-9 sample exhibits the approximate linear lines with sharp triangular shapes at low and at high current densities. The above resultreveals that the JF-9 sample has very good capacitive behavior than all other JF samples [38]. The C_S values was calculated from GCD by the given Eq. (2)

$$Cs = I \times \Delta t/m \times \Delta V \quad (2)$$

Where C_S = specific capacitance (F/g), m is the mass of the active material (g), I = current density (A/g), Δt =charge-discharge time (sec), ΔV = working potential window of the electrode (V/s). The specific capacitance values of GCD is in good agreement with specific capacitance values of CV and it is displayed in Table 2.

P. The above results are proved that the JF-9 electrode material has good charge-discharge rate performance in EDLC.

4.3. Electrochemical impedance spectroscopy

Electrochemical Impedance Spectra (EIS) and the Nyquist plots of the as-prepared porous carbon samples in 1 M Na_2SO_4 electrolytes are shown in Fig. 10. The impedances over a frequency range of 0.1-100 kHz and at open circuit potential of 5 mV. The equivalent circuit diagram of Fig. 10 (depicted inside) includes the resistivity system such as R_s, R_{ct} and W. R_s consists of solution resistance or intrinsic resistance or electrolyte ions resistance or the contact resistance between the active electrode material and current collector. R_{ct} (charge transfer resistance) and W (Warburg resistance). The equivalent circuit, not only exhibits the resistivity system and also displays the capacitance for the system, (i.e.) C_{dl} and it represents the double layer capacitor. In the high-frequency region, the Nyquist plot is semicircle and the real axis intercept is the equivalent series resistance (ESR) [39]. ESR is equal to the difference between the solution resistance (R_s) and charge-transfer resistance (R_{ct}) of the Nyquist plot. The width of the semi-circle impedance loop directly related with charge transfer resistance in the electrode materials. As shown in Fig. 10, all the four curves have nearly the same first point of intersection with the horizontal axis, because all the measurements were carried out using 1M Na_2SO_4 as electrolyte and the same assembly was used for all JFW derived porous carbon samples. It concludes, the resistance caused by the electrolyte and the contact resistance of these electrodes were similar. The second intersection points of the semicircles and the horizontal axis show the inner resistances (ESR). In the low frequency region, the Nyquist plot is a straight line for EDLC. The more vertical line shows the more ideal capacitive behavior [40]. The inset graph of Fig. 10 shows that there is an apparent semi-circle in the high-frequency range in the EIS spectrogram of JF-9 porous nanocarbon electrodes. The above improvment caused by the electric double-layer capacitance with respect to the charge transfer resistance. The R_s and R_{ct} resistance value of JF-9 electrode were 4.72 Ω and 0.76 Ω, indicting a low system resistance and good charge-transfer rate. The indirect line of the low-frequency region represents the ion diffusion resistance process and the degree of ideal supercapacitor is 90°. It can be seen that there is an almost vertical line of JF-9 electrode in the low frequency region, demonstrating that JF 9 electrode had ideal supercapacitive behaviors than all other samples [41,42].

4.4. Effect of current density and cyclic stability

Fig. 11a shows the different current density with the specific capacitance values of Jackfruit derived porous carbon samples. The C_S value increases at the rate of current density decreases as show in Table 2.Hence, the supercapacitor retains a high specific capacitance at a high current density values. Evidently, Table 2 depicts JF-9 sample has 294 F/g at the high current density of 5 A/g and at low current densitiy values (320 F/g at 1 A/g). Thespecific capacitance values of JF-9 results indicated that, at lower current density attains the higher charge discharge time intervals due to stronger interaction at double layer interface between the electrode and electrolytes [43].

Fig. 11b shows the cyclic stability of Jackfruit derived carbon (JF 6, JF 7, JF 8 and JF 9) samples tested at a current density of 1 A/g for 5000 cycles and potential window maintained from 0 to 0.68 V in 1 M Na_2SO_4 electrolyte. From Fig. 11b, JF-9 sample indicates that there is no specific capacitance loss occurs after 5000 cycles and all other sample shows small loss in specific capacitance after 3500 cycles. The capacitance retention obtained for JF-9 is 93%, which strongly demonstrates the excellent electrochemical stability of the electrode material.

The result indicates that the specific capacitance increases when the scanrate decreases and Table 2 evidently matches with the Fig. 11a. It clearly explains that the JF-9 sample has higher specific capacitance at lower scan rate and the specific capacitance is gradually dropped after 75 mV/s. JF-9 has high multi micro and mesoporous structure is the cause for interface reaction between the electrode and electrolyte ions. The ion diffusion between the electrode and electrolyte interface much faster in JF-9 sample than all other porous nanocarbon (JF-8, JF-7 and JF-6) samples. Table 3 shows the comparative supercapcaitor and surface area values of different route prepared activated carbon samples. For comparison study, the specific-capacitance values of modified carbon based electrode materials prepared by other activation methods from various naturally waste organic precursors are listed in Table 3. For the comparison purpose, the similar potential window (0-0.68V) of reported specific capacitance of various precursor route prepared porous carbon are tabulated in Table 3. Comparatively, our preparation

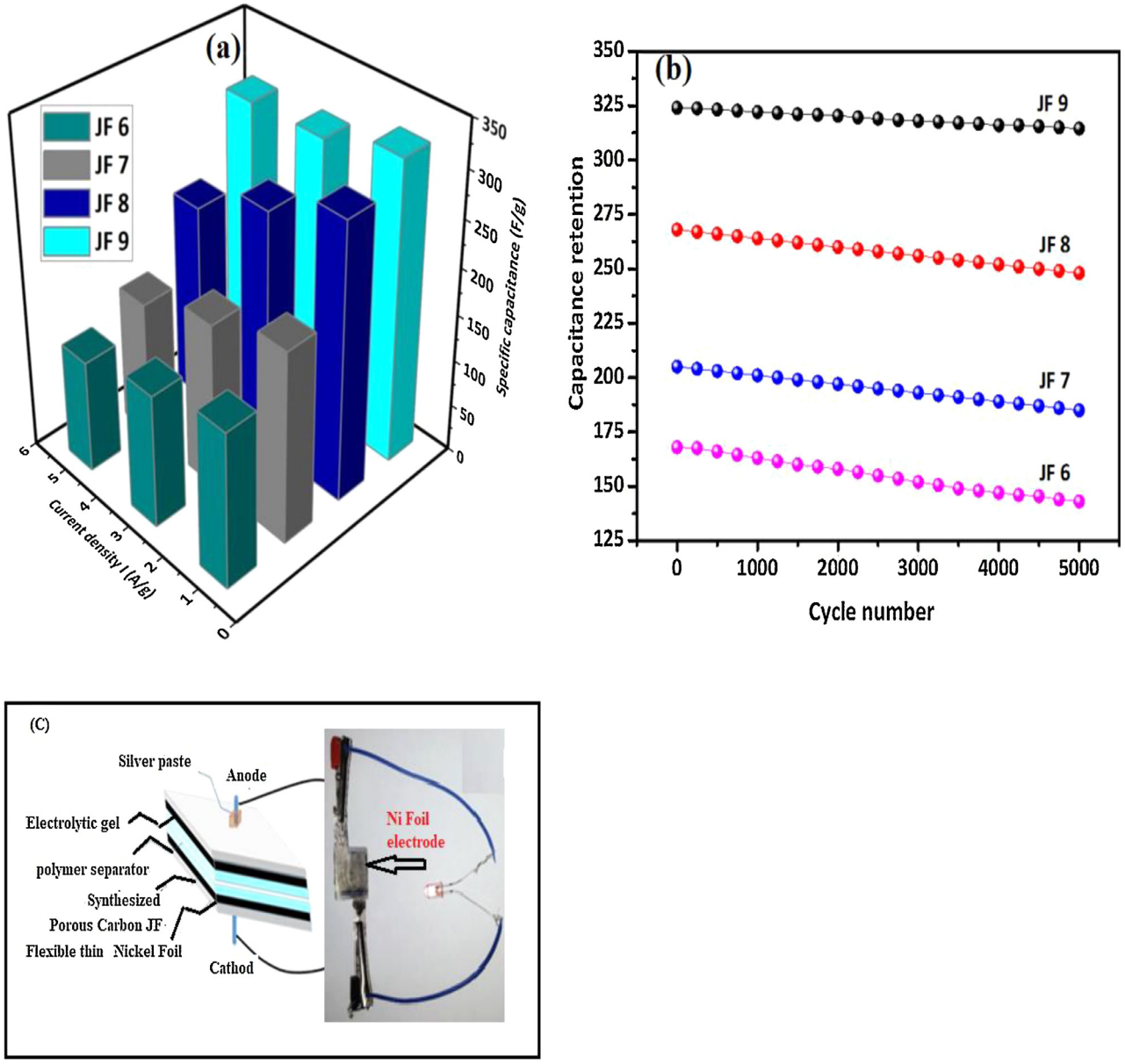

Fig. 11. (a) Specific capacitance Vs current density at different scan rates (1, 3 and 5 A/g) of JF waste derived porous activated carbon samples. (b) Effective Cyclic Stability of as prepared porous carbon from Jackfruit waste (c) Thin flexible Nickel foil electrode setup for JF based porous carbon towards supercapcitor application.

methods are higher yield for fabrication of activated carbon prepared by than inert atmospheric tubular furnaces and microwave methods. Adopting clay molded graphite crucible (CMGC) method is economic way of creating vacuum condition to prepared high yield for carbon formation.

5. Conclusion

Low-cost naturally available Jackfruit peel waste were used as a carbon source to prepare the new porous nanocarbon material by modified pyrolysis method using clay molded graphite crucibles. The porous nanocarbon material was synthesized by a simple and facile chemical activation process using H_3PO_4 followed by heating process by low cost clay mold technique. The specific capacitance of JF-9 was 324 F/g at 5 mV/s in a three electrode electrochemical setup using 1 M Na_2SO_4. The improved higher specific capacitance with excellent long-term cyclic stability (5000 cycles) has occurred, due to improved specific surface area values (1585 m^2/g). In future, Thin Nickel foil based JF derived porous carbon based modified electrode could be used as flexible electrode device for supercapcitor application. In comparison with other reported literature, our method prepared Jackfruit derived carbon exists with micro and mesoporous property obtained below 20 nm pore size distribution with good surface area values.

Declaration of Competing Interest

The authors declare that they have no known competing financial interests or personal relationships that could have appeared to influence the work reported in this paper.

Acknowledgement

The authors acknowledge the financial support through Researchers Supporting Project number (**RSP-2020/54**), King Saud university, Riyadh, Saudi Arabia. Authors (J.J and M.S) acknowledge the management of Loyola College, Chennai, India. M. Sivachidambaram

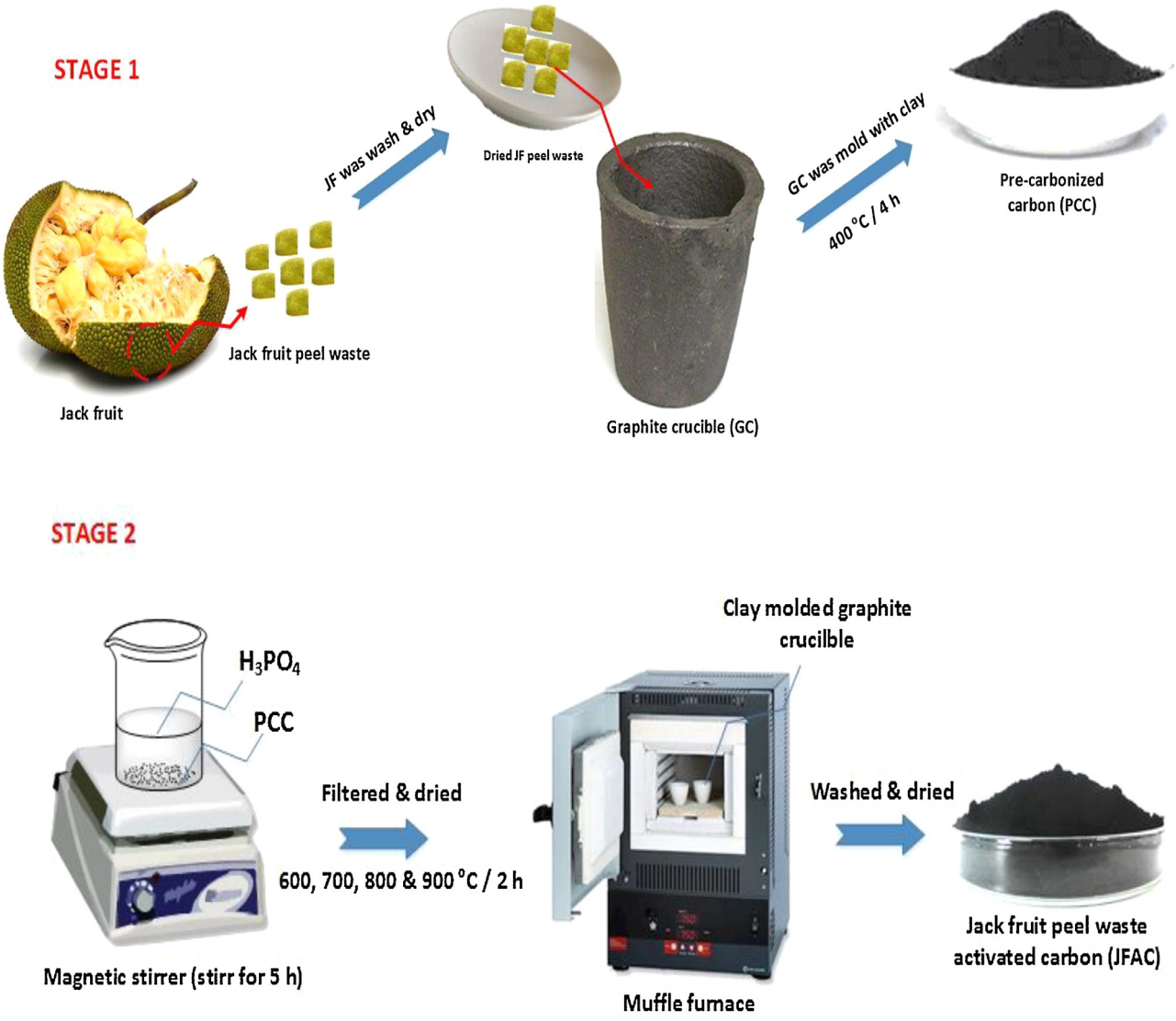

Scheme 1. Schematic diagram for the preparation of JFW porous nanocarbon by Clay Molded Graphite Crucible method.

Table 3.
Comparison of specific capacitance (C_{sp}) of activated porous carbon electrode prepared from various naturally waste organic resource.

Biomass precursors	Activating agent	S_{BET} (m^2/g)	C_{sp} (F/g)	Current density (A/g)	Electrolyte	Reference*
Sugarcane bagasse	$ZnCl_2$	1788	300	0.25	1M H_2SO_4	[44]
Rice husk	$ZnCl_2$	1442	243	0.05	6M KOH	[45]
Human hair	KOH	1104	264	0.25	6M KOH	[46]
Scrap waste tires	H_3PO_4	563	106	1	6M KOH	[47]
Paulownia flower	KOH	1471	297	1	1M H_2SO_4	[48]
Corn cob	HNO_3	543	221	0.5	0.5M H_2SO_4	[49]
Jack fruit peel waste	H_3PO_4	1585	324	1	1M Na_2SO_4	**Present work**

*The similar potential window are taken for the comparison of the capacitance values of previous report

acknowledges DST FIST- 'O' level Centralised Instrumentation Laboratory, Department of chemistry, Theivanai Ammal College for Women, Villupuram. India.

References

[1] X. Chen, C. Li, M. Grätzel, R. Kostecki, S.S. Mao, Nanomaterials for renewable energy production and storage, Chem. Soc. Rev. 41 (2012) 7909, https://doi.org/10.1039/c2cs35230c.
[2] X. Zhang, Y. Li, G. Li, C. Hu, Preparation of Fe/activated carbon directly from rice husk pyrolytic carbon and its application in catalytic hydroxylation of phenol, RSC Adv. 5 (2015) 4984–4992, https://doi.org/10.1039/C4RA13248C.
[3] S. Dutta, A. Bhaumik, K.C.-W. Wu, Hierarchically porous carbon derived from polymers and biomass: effect of interconnected pores on energy applications, Energy Environ. Sci. 7 (2014) 3574–3592, https://doi.org/10.1039/C4EE01075B.
[4] Y. Guo, J. Qi, Y. Jiang, S. Yang, Z. Wang, H. Xu, Performance of electrical double layer capacitors with porous carbons derived from rice husk, Mater. Chem. Phys. 80 (2003) 704–709, https://doi.org/10.1016/S0254-0584(03)00105-6.
[5] D. Hulicova, J. Yamashita, Y. Soneda, H. Hatori, M. Kodama, Supercapacitors prepared from melamine-based carbon, Chem. Mater. 17 (2005) 1241–1247, https://doi.org/10.1021/cm049337g.
[6] A.E. Ismanto, S. Wang, F.E. Soetaredjo, S. Ismadji, Preparation of capacitor's electrode from cassava peel waste, Bioresour. Technol. 101 (2010) 3534–3540, https://doi.org/10.1016/j.biortech.2009.12.123.

[7] Y.-J. Kim, B.-J. Lee, H. Suezaki, T. Chino, Y. Abe, T. Yanagiura, K.C. Park, M. Endo, Preparation and characterization of bamboo-based activated carbons as electrode materials for electric double layer capacitors, Carbon N. Y. 44 (2006) 1592–1595, https://doi.org/10.1016/j.carbon.2006.02.011.

[8] X. Li, W. Xing, S. Zhuo, J. Zhou, F. Li, S.Z. Qiao, G.Q. Lu, Preparation of capacitor's electrode from sunflower seed shell, Bioresour. Technol. 102 (2011) 1118–1123, https://doi.org/10.1016/j.biortech.2010.08.110.

[9] L. Hu, Y. Cui, Energy and environmental nanotechnology in conductive paper and textiles, Energy Environ. Sci. 5 (2012) 6423, https://doi.org/10.1039/c2ee02414d.

[10] L. Xu, M. Jia, Y. Li, S. Zhang, X. Jin, Design and synthesis of graphene/activated carbon/polypyrrole flexible supercapacitor electrodes, RSC Adv. 7 (2017) 31342–31351, https://doi.org/10.1039/C7RA04566B.

[11] Z. Wang, Y. Tan, Y. Yang, X. Zhao, Ying Liu, L. Niu, B. Tichnell, L. Kong, L. Kang, Z. Liu, F. Ran, Pomelo peels-derived porous activated carbon microsheets dual-doped with nitrogen and phosphorus for high performance electrochemical capacitors, J. Power Sourc. 378 (2018) 499–510.

[12] S. Shen, X. Xia, Y Zhong, S Deng, D Xie, B Liu, Y1 Zhang, G Pan, X Wang, J Tu, Implanting niobium carbide into trichoderma spore carbon: a new advanced host for sulfur cathodes, Adv. Mater. 31 (2019) 1900009.

[13] Shenghui Shen, Rongfan Zhou, Yahao Li, Bo Liu, Guoxiang Pan, Qi Liu, Qinqin Xiong, Xiuli Wang, Xinhui Xia, Jiangping Tu, Bacterium, Fungus, and Virus Microorganisms for energy storage and conversion, Small Methods 3 (2019) 1900596.

[14] Yu Zhong, Xinhui Xia, Shengjue Deng, Dong Xie, Shenghui Shen, Kaili Zhang, Weihao Guo, Xiuli Wang, Jiangping Tu, Spore carbon from aspergillus oryzae for advanced electrochemical energy storage, Adv. Mater. 30 (2018) 1805165.

[15] G.Liu Y.Shi, R. Jin, H. Xu, Q. Wang, S. Gao, Carbon materials from melamine sponges for supercapacitors and lithium battery electrode materials: a review, Carbon Energy 1 (2) (2019) 253–275.

[16] B.S. Inbaraj, N. Sulochana, Carbonised jackfruit peel as an adsorbent for the removal of Cd(II) from aqueous solution, Bioresour. Technol. 94 (2004) 49–52, https://doi.org/10.1016/j.biortech.2003.11.018.

[17] S. Xiong, J. Fan, Y. Wang, J. Zhu, J. Yu, Z. Hu, A facile template approach to nitrogen-doped hierarchical porous carbon nanospheres from polydopamine for high-performance supercapacitors, J. Mater. Chem. A. (2017), https://doi.org/10.1039/C7TA05880B.

[18] M. Sivachidambaram, J.J. Vijaya, L.J. Kennedy, R. Jothiramalingam, H.A. Al-Lohedan, M.A. Munusamy, E. Elanthamilan, J.P. Merlin, Preparation and characterization of activated carbon derived from the Borassus flabellifer flower as an electrode material for supercapacitor applications, New J. Chem. 41 (2017) 3939–3949, https://doi.org/10.1039/C6NJ03867K.

[19] Guiyin Xu, Jinpeng Han, Bing Ding, Ping Nie, Jin Pan, Hui Dou, Hongsen Lia, Xiaogang Zhang, Biomass-derived porous carbon materials with sulfur and nitrogen dual-doping for energy storage, Green Chem. 17 (3) (2015) 1668–1674.

[20] Jiahui Li, Binglong Rui, Wenxian Wei, Ping Nie, Limin Chang, Zaiyuan Le, Meiqi Liu, Hairui Wang, Limin Wang, Xiaogang Zhang, Nanosheets assembled layered MoS_2/MXene as high performance anode materials for potassium ion batteries, J. Power Sourc. 449 (15 February 2020) 227481.

[21] Z. Al-Qodah, R. Shawabkah, Production and characterization of granular activated carbon from activated sludge, Braz. J. Chem. Eng. 26 (2009) 127–136.

[22] L. Qie, W. Chen, H. Xu, X. Xiong, Y. Jiang, F. Zou, X. Hu, Y. Xin, Z. Zhang, Y. Huang, Synthesis of functionalized 3D hierarchical porous carbon for high-performance supercapacitors, Energy Environ. Sci. 6 (2013) 2497, https://doi.org/10.1039/c3ee41638k.

[23] Z. Al-Qodah, R. Shawabkah, Production and characterization of granular activated carbon from activated sludge, Braz. J. Chem. Eng. 26 (2009) 127–136, https://doi.org/10.1590/S0104-66322009000100012.

[24] S. Bourbigot, M. Le Bras, R. Delobel, P. Bréant, J. michel Trémillon, Carbonization mechanisms resulting from intumescence-Part II. Association with an ethylene terpolymer and the ammonium polyphosphate-pentaerythritol fire retardant system, Carbon N. Y. 33 (1995) 283–294, https://doi.org/10.1016/0008-6223(94)00131-I.

[25] T.K. Enock, C.K. King'ondu, A. Pogrebnoi, Y.A.C. Jande, Biogas-slurry derived mesoporous carbon for supercapacitor applications, Mater. Today Energy 5 (2017) 126–137, https://doi.org/10.1016/j.mtener.2017.06.006.

[26] Atef S. Alzaydien, Physical, chemical and adsorptive characteristics of local oak sawdust based activated carbons, Asian J. Sci. Res. 9 (2) (2016) 45–56.

[27] Y. Cao, K. Wang, X. Wang, Z. Gu, Q. Fan, W. Gibbons, J.D. Hoefelmeyer, P.R. Kharel, M. Shrestha, Hierarchical porous activated carbon for supercapacitor derived from corn stalk core by potassium hydroxide activation, Electrochim. Acta 212 (2016) 839–847, https://doi.org/10.1016/j.electacta.2016.07.069.

[28] K.S.W. Sing, D.H. Everett, R.A.W. Haul, L. Moscou, R.S. Pierotti, J. Rouquerol, T. Siemieniewska, International union of pure commission on colloid and surface chemistry including catalysis-reporting physisorption data for gas/solid systems with special reference to the determination of surface area and porosity, Pure Appl. Chem. 57 (1985) 603–619, https://doi.org/10.1351/pac198557040603.

[29] C. Vix-Guterl, E. Frackowiak, K. Jurewicz, M. Friebe, J. Parmentier, F. Béguin, Electrochemical energy storage in ordered porous carbon materials, Carbon N. Y. 43 (2005) 1293–1302, https://doi.org/10.1016/j.carbon.2004.12.028.

[30] Y. Han, N. Shen, S. Zhang, D. Li, X. Li, Fish gill-derived activated carbon for supercapacitor application, J. Alloys Compd. 694 (2017) 636–642, https://doi.org/10.1016/j.jallcom.2016.10.013.

[31] L. Sun, C. Wang, Y. Zhou, X. Zhang, J. Qiu, KOH-activated depleted fullerene soot for electrochemical double-layer capacitors, J. Appl. Electrochem. 44 (2014) 309–316, https://doi.org/10.1007/s10800-013-0636-0.

[32] D. Kang, Q. Liu, J. Gu, Y. Su, W. Zhang, D. Zhang, Egg-Box-assisted fabrication of porous carbon with small mesopores for high-rate electric double layer capacitors, ACS Nano 9 (2015) 11225–11233, https://doi.org/10.1021/acsnano.5b04821.

[33] D. Wu, X. Chen, S. Lu, Y. Liang, F. Xu, R. Fu, Study on synergistic effect of ordered mesoporous carbon and carbon aerogel during electrochemical charge-discharge process, Microporous Mesoporous Mater. 131 (2010) 261–264, https://doi.org/10.1016/j.micromeso.2009.12.032.

[34] B. Fang, L. Binder, A modified activated carbon aerogel for high-energy storage in electric double layer capacitors, J. Power Sourc. 163 (2006) 616–622, https://doi.org/10.1016/j.jpowsour.2006.09.014.

[35] Y. Wang, H. Xuan, G. Lin, F. Wang, Z. Chen, X. Dong, A melamine-assisted chemical blowing synthesis of N-doped activated carbon sheets for supercapacitor application, J. Power Sourc. 319 (2016) 262–270, https://doi.org/10.1016/j.jpowsour.2016.04.069.

[36] V. Thongpoola, P. Asanithia, P. Limsuwana, Synthesis of carbon particles using laser ablation in ethanol, Proc. Eng. 32 (2012) 1054–1060.

[37] H. Mi, J. Zhou, Q. Cui, Z. Zhao, C. Yu, X. Wang, J. Qiu, Chemically patterned polyaniline arrays located on pyrolytic graphene for supercapacitors, Carbon N.Y. 80 (2014) 799–807, https://doi.org/10.1016/j.carbon.2014.09.036.

[38] M. Wu, P. Li, Y. Li, J. Liu, Y. Wang, Enteromorpha based porous carbons activated by zinc chloride for supercapacitors with high capacity retention, RSC Adv. 5 (2015) 16575–16581, https://doi.org/10.1039/C4RA13428A.

[39] X. Tian, S. Zhu, J. Peng, Y. Zuo, G. Wang, X. Guo, N. Zhao, Y. Ma, L. Ma, Synthesis of micro- and meso-porous carbon derived from cellulose as an electrode material for supercapacitors, Electrochim. Acta 241 (2017) 170–178, https://doi.org/10.1016/j.electacta.2017.04.038.

[40] X. Tian, H. Ma, Z. Li, S. Yan, L. Ma, F. Yu, G. Wang, X. Guo, Y. Ma, C. Wong, Flute type micropores activated carbon from cotton stalk for high performance supercapacitors, J. Power Sourc. 359 (2017) 88–96. 10.1016/j.jpowsour.2017.05.054. 179.

[41] K. Xia, Q. Gao, J. Jiang, J. Hu, Hierarchical porous carbons with controlled micropores and mesopores for supercapacitor electrode materials, Carbon N. Y. 46 (2008) 1718–1726, https://doi.org/10.1016/j.carbon.2008.07.018.

[42] A.C. Lua, T. Yang, Effect of activation temperature on the textural and chemical properties of potassium hydroxide activated carbon prepared from pistachio-nut shell, J. Colloid Interface Sci. 274 (2004) 594–601, https://doi.org/10.1016/j.jcis.2003.10.001.

[43] W. Li, Y. Ding, W. Zhang, Y. Shu, L. Zhang, F. Yang, Y. Shen, Lignocellulosic biomass for ethanol production and preparation of activated carbon applied for supercapacitor, J. Taiwan Inst. Chem. Eng. 64 (2016) 166–172, https://doi.org/10.1016/j.jtice.2016.04.010.

[44] T.E. Rufford, D. Hulicova-Jurcakova, K. Khosla, Z. Zhu, G.Q. Lu, Microstructure and electrochemical double-layer capacitance of carbon electrodes prepared by zinc chloride activation of sugar cane bagasse, J. Power Sourc. 195 (2010) 912–918, https://doi.org/10.1016/j.jpowsour.2009.08.048.

[45] B.C. Saha, N.N. Nichols, M.A. Cotta, Ethanol production from wheat straw by recombinant Escherichia coli strain FBR5 at high solid loading, Bioresour. Technol. 102 (2011) 10892–10897, https://doi.org/10.1016/j.biortech.2011.09.041.

[46] M. Sevilla, R. Mokaya, Energy storage applications of activated carbons:supercapacitors and hydrogen storage, Energy Environ. Sci 7 (2014) 1250–1280, https://doi.org/10.1039/C3EE43525C.

[47] X. Wang, X. Liang, Y. Wang, X. Wang, M. Liu, D. Yin, S. Xia, J. Zhao, Y. Zhang, Adsorption of copper (II) onto activated carbons from sewage sludge by microwave-induced phosphoric acid and zinc chloride activation, Desalination 278 (2011) 231–237, https://doi.org/10.1016/j.desal.2011.05.033.

[48] D. Yuan, J. Chen, S. Tan, N. Xia, Y. Liu, Worm-like mesoporous carbon synthesized from metal-organic coordination polymers for supercapacitors, Electrochem. Commun. 11 (2009) 1191–1194, https://doi.org/10.1016/j.elecom.2009.03.045.

[49] M. Zhi, F. Yang, F. Meng, M. Li, A. Manivannan, N.N. Wu, Effects of pore structure on performance of an activated-carbon supercapacitor electrode recycled from scrap waste tire, ACS Sustain. Chem. Eng. 2 (2014) 1592–1598, https://doi.org/10.1021/sc500336h.